JBMR Plus, 2024, **8**, 1–12
https://doi.org/10.1093/jbmrpl/ziad014
Advance access publication: January 4 2024
Research Article

Mer tyrosine kinase regulates bone metabolism, and its deficiency partially ameliorates periodontitis- and ovariectomy-induced bone loss in mice

Ka-Young Ryu[1,†], Nitin Kumar Pokhrel[1,†], Hye-Jin Jung[1,†], Hyo Jeong Kim[1], Jiwon Seok[1], Tae-Young Kim[1], Hyung Joon Kim[2], Ji Hye Lee[3], Jae-Young Kim[1], Yong-Gun Kim[4], Youngkyun Lee[1,*]

[1]Department of Biochemistry, School of Dentistry, Kyungpook National University, Daegu 41940, Korea
[2]Department of Oral Physiology, School of Dentistry, Pusan National University, Yangsan 50612, Korea
[3]Department of Oral Pathology, School of Dentistry, Pusan National University, Yangsan 50612, Korea
[4]Department of Periodontology, School of Dentistry, Kyungpook National University, Daegu 41940, Korea
*Corresponding author: Youngkyun Lee, Department of Biochemistry, School of Dentistry, Kyungpook National University, 2177 Dalgubeol-daero, Jung-gu, Daegu 41940, South Korea (ylee@knu.ac.kr).
[†]These authors contributed equally to this work.

Abstract

Bone homeostasis is maintained by tightly coordinated activities of bone-forming osteoblasts and bone-resorbing osteoclasts. In the present report, the role of Mer tyrosine kinase (MerTK) in bone metabolism was investigated. The expression of MerTK decreased upon BMP2 stimulation of osteoblast precursors. The femurs of *Mertk*-deficient mice showed significantly increased bone volume with concomitant increase of bone formation and reduction in bone resorption. These bone phenotypes were attributed to the increased osteoblast differentiation and mineralization accounted by the enhanced β-catenin and Smad signaling in the absence of MerTK in osteoblast precursors. Although the *Mertk*-deficient bone marrow macrophages were predisposed to enhanced osteoclast differentiation via augmented Ca^{2+}-NFATc1 signaling, the dramatic increase of *Tnfsf11b/Tnfsf11* (*Opg/Rankl*) ratio in *Mertk* knockout bones and osteoblast precursors corroborated the reduction of osteoclastogenesis in *Mertk* deficiency. In ligature-induced periodontitis and ovariectomy models, the bone resorption was significantly attenuated in *Mertk*-deficient mice compared with wild-type control. Taken together, these data indicate novel role of MerTK in bone metabolism and suggest a potential strategy targeting MerTK in treating bone-lytic diseases including periodontitis and osteoporosis.

Keywords: osteoclasts, osteoblasts, bone metabolism, periodontitis, ovariectomy

Graphical Abstract

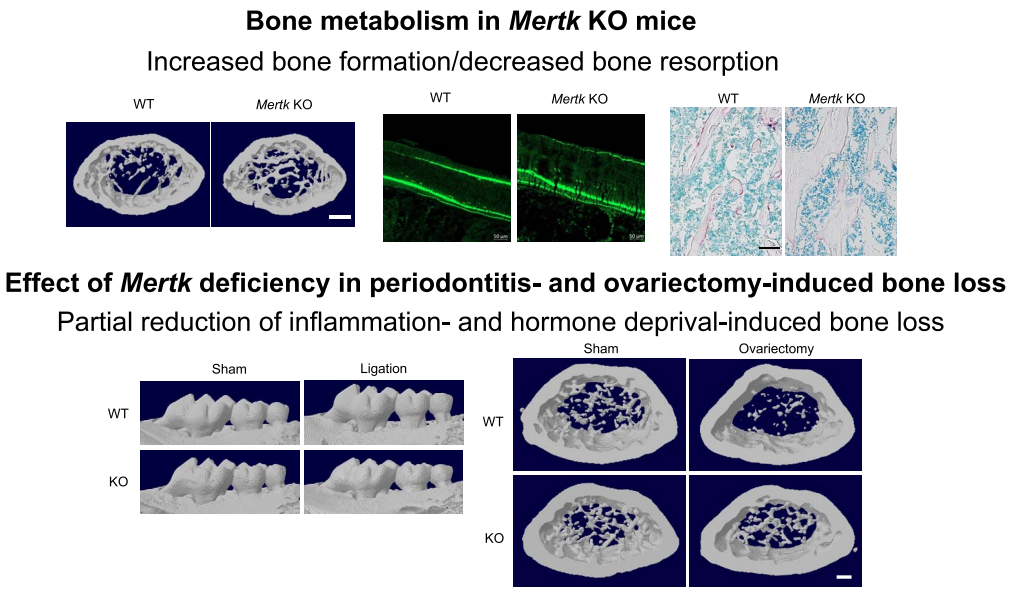

Received: July 31, 2023. **Revised:** November 22, 2023. **Accepted:** December 11, 2023

Introduction

Bone is a dynamic tissue that old bones are constantly removed and replaced by new bones. Bone homeostasis is maintained by a precisely coordinated actions of bone-forming osteoblasts and bone-resorbing osteoclasts through a process called bone remodeling.[1] Both systemic and local hormones, growth factors, and cytokines consist of a tight regulatory network to preserve skeletal integrity.[2] In addition, the balance between receptor activator of nuclear factor κB ligand (RANKL) and osteoprotegerin (OPG) produced by osteoblast lineage cells determine the extent of osteoclastogenesis,[3–7] coupling the differentiation and activities of these two cells that regulate bone metabolism. The imbalance of bone formation and resorption, for example, excessive osteoclastogenesis, is often observed in many skeletal diseases such as osteoporosis, rheumatoid arthritis, and periodontitis. In periodontitis, persistent inflammatory conditions stimulate osteoclast differentiation and function, leading to significant resorption of alveolar bones[8,9] that ultimately contributes to the loss of tooth.[10,11]

Mer tyrosine kinase (MerTK) is a member of TAM receptor tyrosine kinase family named after the constituents Tyro3, Axl, and MerTK.[12] The biological function of MerTK is largely elucidated by the phenotype of mice that bear loss-of-function mutation. Although the *Mertk* knockout (KO) mice are viable and fertile, they exhibited susceptibility to LPS-induced endotoxic shock[13] and retinal dystrophy due to the failure of phagocytosis by retinal pigment epithelium cells,[14] suggesting its role in immune regulation and phagocytosis of apoptotic cells.[12] Indeed, the *Mertk* KO macrophages had defects in clearing apoptotic thymocytes.[15] In addition, recent studies suggest an involvement of MerTK in carcinogenesis and suppression of anti-tumor immunity.[16]

In the present study, the role of MerTK in bone metabolism is reported for the first time by analyzing the bone phenotype of *Mertk* KO mice. The *Mertk* deficiency induced increased bone formation and osteoblast differentiation, while reducing the osteoblast-dependent osteoclastogenesis and bone resorption. These data not only suggest a novel role of MerTK in bone metabolism but also provide a potential therapeutic opportunity for bone-lytic diseases including periodontitis and osteoporosis.

Materials and methods

Animals

The B6;129-*Mertk*^{tm1Grl}/J (Jax:011122) mice that harbor deletion in exon 18 of *Mertk* gene[17] were purchased from the Jackson Laboratory (Bar Harbor, ME, USA). These mice were bred with C57BL6/J mice (Central Lab. Animal Inc., Seoul, Korea) for 6 generations before maintaining colony by crossing heterozygous males and females. Littermate wild-type (WT) mice were used as controls. Mice were housed in a specific pathogen-free facility with controlled temperature, humidity, light/dark cycle, and free access to standard rodent chow and tap water. All animal protocols were approved by the committees on the care and use of animal research at Kyungpook National University (KNU 2020-0056) and followed the guidelines of Animal Research: Reporting of In Vivo Research.[18]

Antibodies and reagents

Recombinant human RANKL and M-CSF were obtained from PeproTech (Cranbury, NJ, USA). Recombinant human/-mouse/rat BMP-2 (355-BM) was purchased from R&D Systems (Minneapolis, MN, USA). Anti-mouse MerTK antibody (AF591) was from R&D Systems. Anti-Samd1 (9743), phospho-Smad1/5/8 (9511), β-catenin (9562), GSK3β (12456), phospho-GSK3β (5558, Ser 9), and NF-κB (8242) antibodies were from Cell Signaling Technology (Danvers, MA, USA). Anti-NFATc1 antibody (7A6) was purchased from BD Biosciences Pharmingen (San Diego, CA, USA). Anti-Lamin B (M-20) was obtained from Santa Cruz Biotechnology (Dallas, TX, USA). Anti-Osteocalcin antibody (ALX-210-333) was from Enzo Lifesciences (Farmingdale, NY, USA). Antibody against Osteoprotegerin (A2100) was purchased from ABclonal (Woburn, MA, USA). Anti-β-actin was obtained from Sigma-Aldrich (St. Louis, MO, USA). All other reagents were purchased from Sigma-Aldrich unless otherwise specified.

Osteoblast differentiation

The calvarial cells were isolated by digesting calvariae of newborn mice using 0.1% collagenase (type IA-S from *Clostridium histolyticum*; Sigma) and 0.2% Dispase II neutral protease (grade II; Roche, Basel, Switzerland). These cells were seeded at a density of 10^4/well in 48-well tissue culture plates in α-MEM (Welgene, Daegu, Korea) supplemented with 10% FBS (Thermo Fisher Scientific, Waltham, MA, USA) and were further stimulated with 30 ng/mL BMP-2. The osteogenic differentiation and mineralization were confirmed by staining for the alkaline phosphatase (ALP) activity (ALP kit; Sigma) or by alizarin red staining. The cells were observed and photographed under Olympus BX51 microscope equipped with 10 ×, 4 ×, and 1.25 × objective lenses and DP73 digital camera system (Olympus, Center Valley, PA, USA).

RNA isolation and quantitative RT-PCR analysis

Total RNAs were extracted by TRIzol reagent (Thermo Fisher Scientific) and 1 μg of RNA in each sample was reverse transcribed using SuperScript II reverse transcriptase (Thermo Fisher Scientific). The resulting cDNAs in optical tubes (Thermo Fisher Scientific) were amplified using SYBR green master mix (Thermo Fisher Scientific) in an AB7500 real-time PCR instrument (Thermo Fisher Scientific). The relative expression of mRNAs against that of *Hprt1* was calculated using threshold cycle (Ct) values. The primer sequences used were published previously.[19]

Immunoblotting

Cells were lysed in a buffer containing 10 mM Tris, pH 7.2, 150 mM NaCl, 5 mM EDTA, 1 mM NaF, 1 mM Na_3VO_4, 0.1% SDS, 1% Triton X-100, and 1% deoxycholic acid. After separation by SDS-PAGE, proteins were transferred onto nitrocellulose membranes. After blocking followed by incubation with primary and secondary antibodies, the enhanced chemiluminescence signals were detected in Fusion FX system (Vilber Lourmat, Marne La Vallee, France). Blots against β-actin served as loading controls. When multiple blots were performed using aliquots of same lysates, only one representative control blot was shown, although β-actin blots were carried out for every membrane. The densitometry of western blots was performed using Fusion Capt Advance

software (Vilber Lourmat), and the band intensity of each lane was divided by total band intensities of the protein of interest.

Analysis of mouse bone phenotypes

Femurs and lumbar vertebrae were isolated from of 6-week-old male ($n = 7$ per group) and female ($n = 5$ per group) WT and *Mertk* KO mice. All mice were injected with 5 mg/kg calcein i.p. at 10 and 3 d before sacrifice. The femurs were subjected to microcomputed tomography (μCT) analysis followed by sequential decalcification, paraffin embedding, tissue sectioning, and immunohistochemical/histological analyses as described below. The femurs of contralateral side were embedded in methyl methacrylate resin for further analysis of bone histomorphometry. The L4 vertebrae were subjected to μCT analysis.

Microcomputed tomography

Femurs, jaw bones, and vertebrae were fixed in 4% paraformaldehyde and were subjected to μCT analysis in SkyScan 1275 scanner (Bruker, Kontich, Belgium) at 50 kV, 75 μA, 11.7 μm/pixel spatial resolution, 100 ms exposure, 0.2° rotation step, 360° rotation, no frame averaging, and 1-mm Al filter. The 3-dimensional images were reconstructed using CT-volume software (Bruker). The volumetric analysis for bone volume to tissue volume (BV/TV), trabecular thickness (Tb. Th), trabecular number (Tb. N), and trabecular separation (Tb. Sp) of distal femur was performed using the slices spanning 1 mm, along a region at 1 to 2 mm below the lowest point of the growth plate using the CT-analysis program (Bruker). The cortical thickness was measured by volumetric analysis of 1-mm-thick cortical region spanning 2.5 to 3.5 mm below the growth plate. The volumetric analysis of trabecular bones of L4 vertebrae was performed in the approximately 1-mm-thick trabecular region in the vertebral body, between the cranial and caudal growth plates. The representative images of coronal, transverse, and sagittal sections were obtained by Data viewer program (Bruker). The average distance between cemento-enamel junction and alveolar bone crest (CEJ-ABC) was measured at 3 points (mesial cusp, distal cusp, and groove of the second molar) from the reconstructed 3-dimensional images using CT-analysis program (Bruker).[20]

Immunohistochemistry and TRAP staining

Femurs and maxillary tissues were fixed in 4% paraformaldehyde, decalcified in 12% EDTA, and embedded in paraffin. Bone sections of 5 μm thickness were prepared using RM 2245 microtome (Leica Microsystems, Bannockburn, IL, USA). For immunohistological staining of osteoblasts, samples were treated with citrate buffer (pH 6.0) for 15 min at 95 °C followed by 3% H_2O_2 in methanol for 20 min. After blocking with 2.5% horse serum, samples were incubated with anti-Osteocalcin antibody (1:100) or anti-Osteoprotegerin (1:100) overnight at 4 °C followed by secondary antibody (1:1000) for 1 h. Then, the tissues were treated with 3,3′-diaminobenzidine and counterstained with methyl green. For the visualization of osteoclasts, decalcified tissue sections were stained for tartrate-resistant acid phosphatase (TRAP) activity using a leukocyte acid phosphatase kit (Sigma-Aldrich) followed by counterstaining with methyl green.

Bone histomorphometry

The histomorphometric analysis of osteoclasts in femurs for osteoclast number per bone perimeter (N. Oc/B. Pm) and osteoclast surface per bone surface (Oc. S/BS) was performed using Osteomeasure software (OsteoMetrics, Decatur, CA, USA) in the trabecular region beginning 300 μm below the growth plate. The measurement of osteoclasts in alveolar bones was performed using the coronal sections of tissues containing maxillary second molar and surrounding periodontium. The number of osteoblasts per bone perimeter (N. OB/B. Pm) on endocortical surface of femurs was measured from the osteocalcin-stained slides in a region 2 to 4 mm below the growth plate. For the measurement of bone formation, mice were injected with 5 mg/kg calcein twice with 7-d interval. Femurs were fixed and embedded in methyl methacrylate resin. The undecalcified tissue sections of 7 μm thickness were prepared using RM 2245 microtome equipped with tungsten-carbide blades (Leica Microsystems). The calcein fluorescence in the endosteal surface in the mid-diaphysis region (2 to 4 mm below growth plate) was observed under LSM 800 confocal microscope (Carl Zeiss Microscopy, Jena, Germany) furnished with 20 ×/0.45 S Fluor objective lens (Nikon Instruments, Melville, NY). The mineral apposition rate (MAR), single- and double-labelled surface, and mineralizing surface, and bone formation rate (BFR/BS) were measured using the Osteomeasure software. The quantification was carried out in a blinded fashion and was confirmed by at least two researchers. All histomorphometric analyses followed the guidelines by American Society of Bone and Mineral Research.[21]

Osteoclast differentiation

The bone marrow macrophage osteoclast precursors (BMMs) were prepared by treating bone marrow cells flushed from femurs and tibias of 6-wk-old mice with 20 ng/mL M-CSF for 3 d.[19] BMMs were then stimulated with 100 ng/mL RANKL for 3 to 4 d in the presence of 20 ng/mL M-CSF before staining for TRAP activity using a leukocyte acid phosphatase kit (Sigma-Aldrich). For the co-culture experiments with osteoblasts, BMMs (2×10^4) were layered on top of calvarial cells (10^4) in 48-well culture plates and treated with 10 nM vitamin D_3 and 1 μM PGE_2 (Sigma-Aldrich) for 7 d for TRAP staining.

Measurement of intracellular Ca^{2+} oscillations

The BMMs were stimulated with 20 ng/mL M-CSF and 100 ng/mL RANKL for 2 d and labeled with 5 μM FLUO4/AM by incubation for 30 min. Cells were washed, resuspended in Locke's buffer (154 mM NaCl, 5.6 mM KCl, 3.6 mM $NaHCO_3$, 1.3 mM $CaCl_2$, 5 mM glucose, 10 mM HEPES, pH 7.4), and observed for 10 min at room temperature under an Eclipse Ti-S fluorescence microscope (Nikon Instruments, Melville, NY, USA) equipped with a Zyla 5.5 sCMOS digital camera (Andor Technology, Belfast, UK). The recorded FLUO4 signals were analyzed by MetaFluor software (Molecular Devices, Sunnyvale, CA, USA).

Immunofluorescence

The BMMs were cultured on 10-mm-diameter glass cover slips (Paul Marienfeld, Lauda-Königshofen, Germany) with M-CSF and RANKL for 2 d. Cells were fixed, permeabilized, and immunostained with anti-Lamin B antibody followed by Alexa Fluor 555–conjugated secondary antibody (Thermo

Fisher Scientific). Cells were further labeled with anti-NFATc1 antibody and Alexa Fluor 488–conjugated secondary antibody and observed under a LSM 5 PASCAL laser scanning microscope (Carl Zeiss, Göttingen, Germany).

Sample size calculation

The number of animals required to get statistically significant results was calculated via power analysis using G*Power 3.1 program (http://www.psychologie.hhu.de). Briefly, the primary outcome for ovariectomy experiments was set as 50% reduction in bone loss by ovariectomy measured by femoral trabecular BV/TV. The mean difference was 0.75% and the SD was 1.60%. The required sample size was calculated to 38 to meet $\alpha = 0.05$ and $1\text{-}\beta = 0.8$. Similarly, the primary outcome for ligature experiments was 50% reduction in alveolar bone loss measured by the CEJ-ABC distance, the mean difference was 37.5 μm, and the SD was 5.72 μm. Then, the required sample size was calculated to 21 to meet $\alpha = 0.05$ and $1\text{-}\beta = 0.8$.

Ligature-induced periodontitis and ovariectomy

Eight-week-old male WT ($n = 11$) and KO mice ($n = 10$) were anesthetized by i.p. injection of 250 mg/kg 2,2,2-tribromoethanol (Sigma-Aldrich) and randomly divided into two groups. Half of the mice in each genotype ($n = 6$ for WT and $n = 5$ for KO) received a silk (6-0, Ailee, Busan, Korea) ligature around the left maxillary second molar to induce periodontitis.[20] The other half of the mice in each genotype ($n = 5$ for WT and KO, respectively) were left unligated and served as sham-operated controls. At 7 d after the operation, mice were euthanized, and the maxillary tissues were isolated for the radiological and histological analyses. Twelve-week-old female WT ($n = 20$) and *Mertk* KO mice ($n = 20$) were anesthetized by i.p. injection (250 mg/kg) of 2,2,2-tribromoethanol. Half of the mice in each genotype ($n = 10$ for WT and KO, respectively) received bilateral ovariectomy. The other half of the mice in each genotype ($n = 10$ for WT and KO, respectively) only received incisions without ovariectomy and served as sham-operated controls. At 4 wk after operation, mice were sacrificed, and tissues were collected for further radiological and histological analyses.

Statistics

All in vitro data including blots and photographs are representative of at least 3 experiments performed in triplicates with similar results unless otherwise specified. All quantitative data were tested for normal distribution by Shapiro-Wilk normality test. To determine the significant difference between experimental groups, one-way or two-way ANOVA followed by Tukey's multiple comparisons or unpaired, two-tailed Student's t test was used. When the data did not follow normal distribution, the significance of difference was examined by Mann-Whitney U test. The P-value $<.05$ was considered significant.

Results

Mertk deficiency increases bone volume in mice

Although the expression of *Mertk* has been reported in a wide range of cells and tissues,[16] the role in skeletal homeostasis is yet to be identified. To explore the potential role of MerTK in osteoblasts, the expression of *Mertk* mRNA was examined in mouse calvarial cells upon BMP2 treatment. As shown in Figure 1A, BMP2 significantly reduced the expression of *Mertk*, most dramatically at 7 d after stimulation. The expression of MerTK protein corroborated the reduced mRNA expression, being conspicuously reduced at day 7 after BMP2 stimulation (Figure 1B). To gain insights into the physiological role of MerTK in bone metabolism, the bone phenotype of *Mertk* KO mice was examined by analyzing the femurs of 6-wk-old male and female WT and KO littermates by μCT. A 3-dimensional reconstruction of the data represented significant increase of trabecular bones in KO femurs compared with WT in male mice (Figure 1C). The trabecular bone parameters including trabecular bone volume, trabecular number, and trabecular separation were significantly higher in KO femurs, while trabecular thickness remained unchanged (Figure 1D-G). The increased trabecular bone density was also observed in female mice, with significantly higher trabecular bone volume, trabecular thickness, and trabecular number in KO mice compared with WT (Supplementary Figure S1A and B). The cortical thickness was significantly higher in male KO mice (Supplementary Figure S1C and D). However, the cortical thickness was not statistically different between WT and KO in females (Supplementary Figure S1E and F). The role of *Mertk* in axial skeletons was also noticeable, with significantly higher trabecular bone volume in the vertebral bodies of KO mice compared with WT in both males and females (Supplementary Figure S1G to J). To further confirm whether these bone phenotypes originated from the increased bone formation, the incorporation of calcein into newly formed bones was examined (Figure 1H). Compared with WT, the distance between 2 calcein labels was wider in KO femurs. In addition, the double-labeled surface was much larger in endocortical surface of KO femurs compared with WT. These results are reflected in significantly higher MAR (Figure 1I) and bone formation rate (Figure 1J) in *Mertk* KO mice compared with WT. Furthermore, immunohistochemical staining indicated distinctively larger surface of osteocalcin-positive cells on KO bones, which were larger and more cuboidal in shape (Figure 1K). The number of osteoblasts was significantly higher in KO femurs compared with WT (Figure 1L). Finally, femoral tissue sections were stained for TRAP activity to assess the effect of *Mertk* deficiency on osteoclastogenesis (Figure 1M). Notably, the number of osteoclasts per bone perimeter was significantly lower in KO femurs compared with WT (Figure 1N). The decrease of osteoclast number was in good accordance with the significantly lower level of serum carboxy-terminal collagen type 1 crosslinks (CTX) in KO mice compared with WT for both males (Figue 1O) and females (Supplementary Figure S1K).

Mertk deficiency increases osteoblast differentiation

To investigate whether MerTK directly regulate osteoblastogenesis, primary calvarial cells isolated from *Mertk* KO and WT mice were stimulated with BMP2 to induce osteogenic differentiation. Staining for the ALP activity in Figure 2A clearly shows that osteoblast differentiation is dramatically enhanced in KO cells compared with WT. In addition, alizarin red staining indicated mineral deposition is also greatly increased in KO calvarial cells upon BMP2 stimulation for 14 d (Figure 2B). The enhanced ALP production and

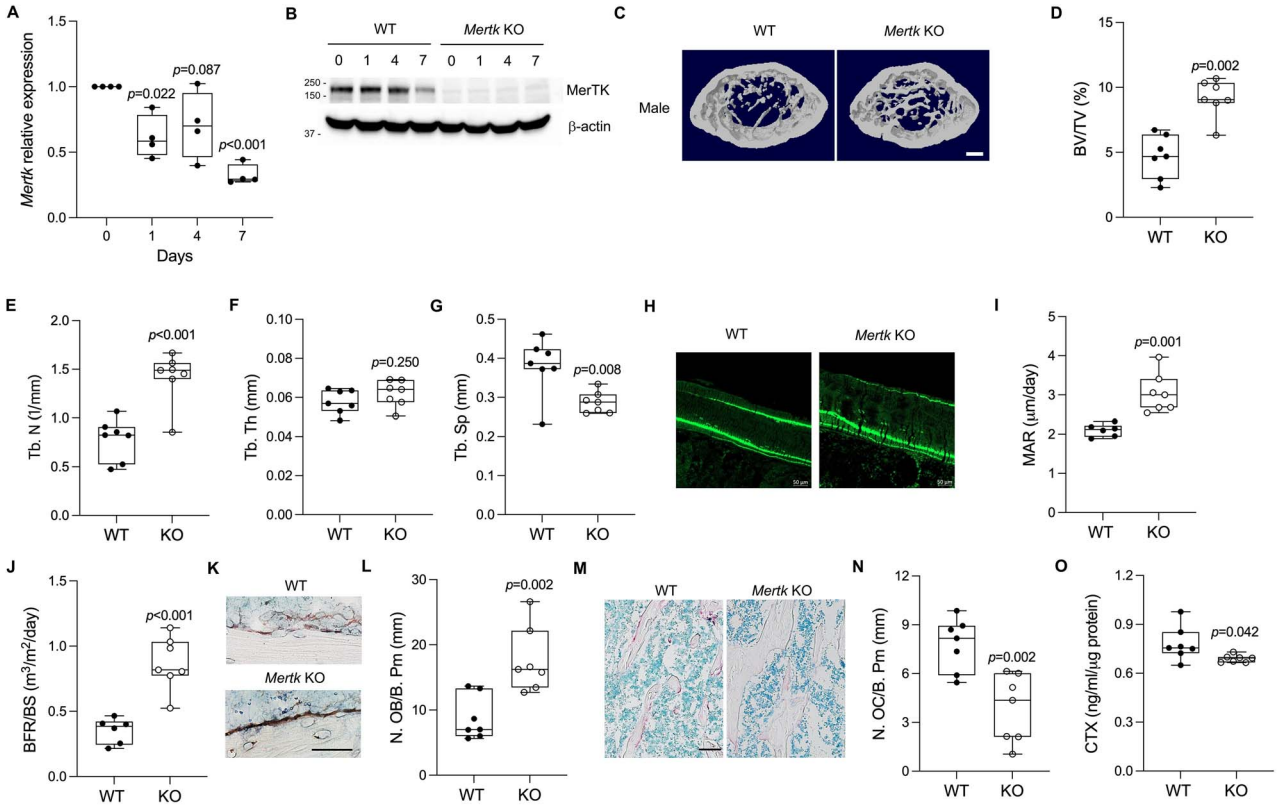

Figure 1. Bone phenotypes of *Mertk* KO mice. (A) Expression of *Mertk* mRNA was measured from mouse calvarial cells treated with 30 ng/mL BMP2 by real-time PCR analysis. The results from 4 independent experiments performed in triplicates are combined, in which relative expression levels to the control cells are shown. The F and *P*-values for one-way ANOVA analysis were 12.41 and <.001, respectively. (B) WT or *Mertk* KO calvarial cells were stimulated with 30 ng/mL BMP2 for 7 d. The expression of MerTK protein was examined by western blot. (C) Distal femurs of 6-wk-old male WT and *Mertk* KO mice were subjected to microcomputed tomography analysis followed by 3-dimensional reconstruction of the data. Scale bar indicates 200 μm. (D to G) Trabecular bone parameters were calculated from the data obtained in (C). (H) After calcein double labeling of 6-wk-old male mice, cortical bones in the diaphysis of femurs were observed under a confocal fluorescence microscope. Scale bar indicates 50 μm. (I and J) The mineral apposition rate and bone formation rate were calculated from the results in (H). (K) The femur sections of 6-wk-old male WT and *Mertk* KO mice were immunostained for Osteocalcin. The cortical area in the mid-diaphysis was shown. Scale bar indicates 50 μm. (L) The number of Osteocalcin-positive osteoblasts per bone perimeter was counted from the results in (K). (M) The femur sections of 6-wk-old male WT and *Mertk* KO mice were stained for TRAP activity. The secondary spongiosa are shown. Scale bar indicates 50 μm. (N) The number of osteoclasts per bone perimeter was counted from the results in (M). (O) The serum CTX levels were examined in 6-wk-old male mice using a CTX-1 ELISA kit. The results were normalized by protein concentrations in the sera.

mineralization by KO calvarial cells was also observed when the cells were cultured in osteogenic media containing β-glycerophosphate, ascorbic acid, and dexamethasone (Supplementary Figure S2A and B). UNC 569, a MerTK inhibitor, potently augmented osteogenic differentiation of calvarial cells (Supplementary Figure S2C and D), further confirming the role of MerTK in osteoblasts. The significantly increased mRNA expression of osteoblast marker genes, such as *Alpl* (Alkaline phosphatase), *Sp7* (Osterix), and *Bglap* (Osteocalcin), in KO calvarial cells after BMP2 stimulation verified the enhanced osteoblast differentiation (Figure 2C). To gain insights into the signaling events leading to the accelerated osteoblastogenesis, the expression and phosphorylation of several key regulators of osteoblast differentiation were examined. The western blot analysis in Figure 2D confirmed that the expression of MerTK significantly decreased during the culture of WT mouse calvarial cells with BMP2 while there was no detectable MerTK protein in KO cells. In these conditions, the β-catenin expression and GSK3β phosphorylation was conspicuously higher in KO calvarial cells compared with WT, as evidenced by densitometry analysis (Figure 2E). In addition, the phosphorylation of Smad1/5/8 and the expression of NFATc1 were also significantly higher in KO cells compared with WT.

Mertk deficiency inhibits osteoblast-dependent osteoclast differentiation

The *Mertk* expression was also detected in BMMs, which sharply decreased upon stimulation of these cells with RANKL (Figure 3A). The expression of MerTK protein in BMMs corroborated the mRNA expression, also decreasing over time following treatment with RANKL for 3 d (Figure 3B). To our surprise, when *Mertk* KO BMMs were stimulated with RANKL, the formation of TRAP-positive osteoclasts was significantly augmented compared with WT controls (Figure 3C and D). In accordance with the enhanced osteoclastogenesis, KO BMMs generated larger resorbed area compared with WT when cells were cultured on dentin discs (Supplementary Figure S3A and B). The enhanced osteoclast differentiation in *Mertk*-deficient cells was accompanied by the increased expression of marker genes for osteoclast differentiation (*Acp5* and *Ctsk*) as well as fusion (*Atp6v0d2* and *Dcstamp*) (Figure 3E). In addition, the expression of NFATc1, a key transcription factor for osteoclastogenesis,

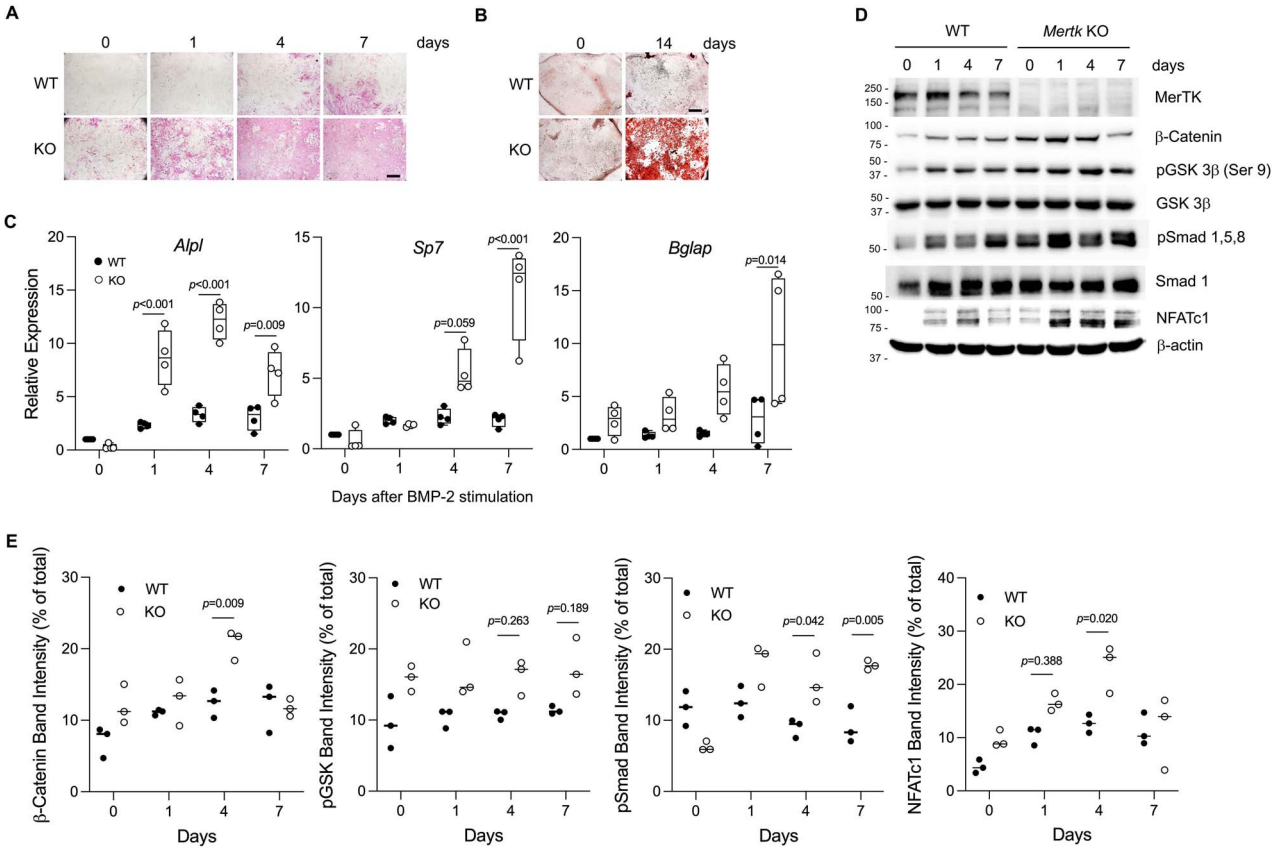

Figure 2. The effect of MerTK deficiency on osteoblast differentiation. (A) Calvarial cells isolated from WT or *Mertk* KO mice were stimulated with 30 ng/mL BMP2 for 7 d. Cells were then stained for alkaline phosphatase activity. Scale bar indicates 2 mm. (B) Calvarial cells were incubated with 30 ng/mL BMP2 for 14 d and subjected to alizarin red staining. Scale bar indicates 2 mm. (C) WT or *Mertk* KO calvarial cells were stimulated with 30 ng/mL BMP2 for 7 d. The mRNA expression levels of alkaline phosphatase (*Alpl*), Osterix (*Sp7*), and Osteocalcin (*Bglap*) were measured by real-time RT-PCR analysis. Data are mean of 4 experiments performed in triplicates. The *P*-values for two-way ANOVA in the order of interaction, genotype, and BMP2 stimulation were *Alpl* (<.001, <.001, <.001), *Sp7* (<.001, <.001, <.001), and *Bglap* (.156, <.001, <.001). (D) Cell lysates in (C) were subjected to western blotting for the expression or phosphorylation of key regulators of osteoblast differentiation. (E) The band intensities in (D) were quantified using results from three independent experiments. The *P*-values for two-way ANOVA in the order of interaction, genotype, and BMP2 stimulation were β-catenin (.027, .002, <.001), pGSK (.991, <.001, .788), pSmad (<.001, <.001, .002), and NFATc1 (.099, <.001, <.001).

was significantly unregulated in KO BMMs compared with WT cells upon RANKL treatment (Figure 3F and Supplementary Figure S3C). However, the NF-κB expression was not significantly affected by *Mertk* deficiency (Supplementary Figure S3D). In an NFATc1 autoamplification model, increased intracellular Ca^{2+} induces nuclear translocation and its own transcription of NFATc1.[22,23] When the Ca^{2+} responses were examined in RANKL-treated BMMs loaded with fluorescent Ca^{2+} indicator, *Mertk* KO cells exhibited significantly more robust Ca^{2+} oscillations compared with WT controls (Figure 3G). The *Mertk*-deficient cells not only manifested significantly higher number of cells with Ca^{2+} oscillations (Supplementary Figure S3E) but also showed higher frequency of Ca^{2+} peaks (Supplementary Figure S3F) and amplitude (Supplementary Figure S3G). Finally, immunofluorescence staining of BMMs after RANKL stimulation demonstrated extensive nuclear NFATc1 localization in KO cells compared with WT (Figure 3H). The proportion of cells showing nuclear NFATc1 expression in *Mertk* KO cells was more than double of that observed in WT BMMs (Figure 3I). The increased expression of nuclear NFATc1 upon RANKL stimulation in *Mertk*-deficient BMMs was further confirmed by western blot analysis of nuclear extracts (Supplementary Figure S3H and I).

Since the increased osteoclast differentiation in vitro contrasted the significantly reduced osteoclast number in bone (Figure 1), the ratio of *Tnfrsf11b*/*Tnfsf11* (*Opg*/*Rankl*) was measured in RNAs isolated from the femurs. Figure 4A shows that the *Tnfrsf11b*/*Tnfsf11* ratio is significantly higher in KO bone, suggesting that the *Mertk* deficiency generates an environment that suppresses osteoclast differentiation. The enhanced Opg expression in *Mertk*-deficient femurs was further confirmed by immunostaining (Supplementary Figure S4A). Interestingly, the Opg expression in the absence of *Mertk* was significantly more conspicuous not only in cells on bone surface but also in cells in lacunae and bone marrow (Supplementary Figure S4B). The *Tnfrsf11b*/*Tnfsf11* ratio in calvarial cells was also significantly higher in *Mertk*-deficient calvarial cells compared with WT (Figure 4B). To test whether the altered balance of *Tnfrsf11b* and *Tnfsf11* regulates osteoclastogenesis, WT and KO osteoclast precursors cells (BMMs) were co-cultured with either WT or KO calvarial cells. When these cells were stimulated with vitamin D_3 and PGE_2, WT calvarial cells efficiently supported the formation of osteoclasts, while KO calvarial cells did not (Figure 4C). The number of osteoclasts generated in the presence of *Mertk* KO calvarial cells was dramatically reduced compared with that by WT calvarial cells regardless

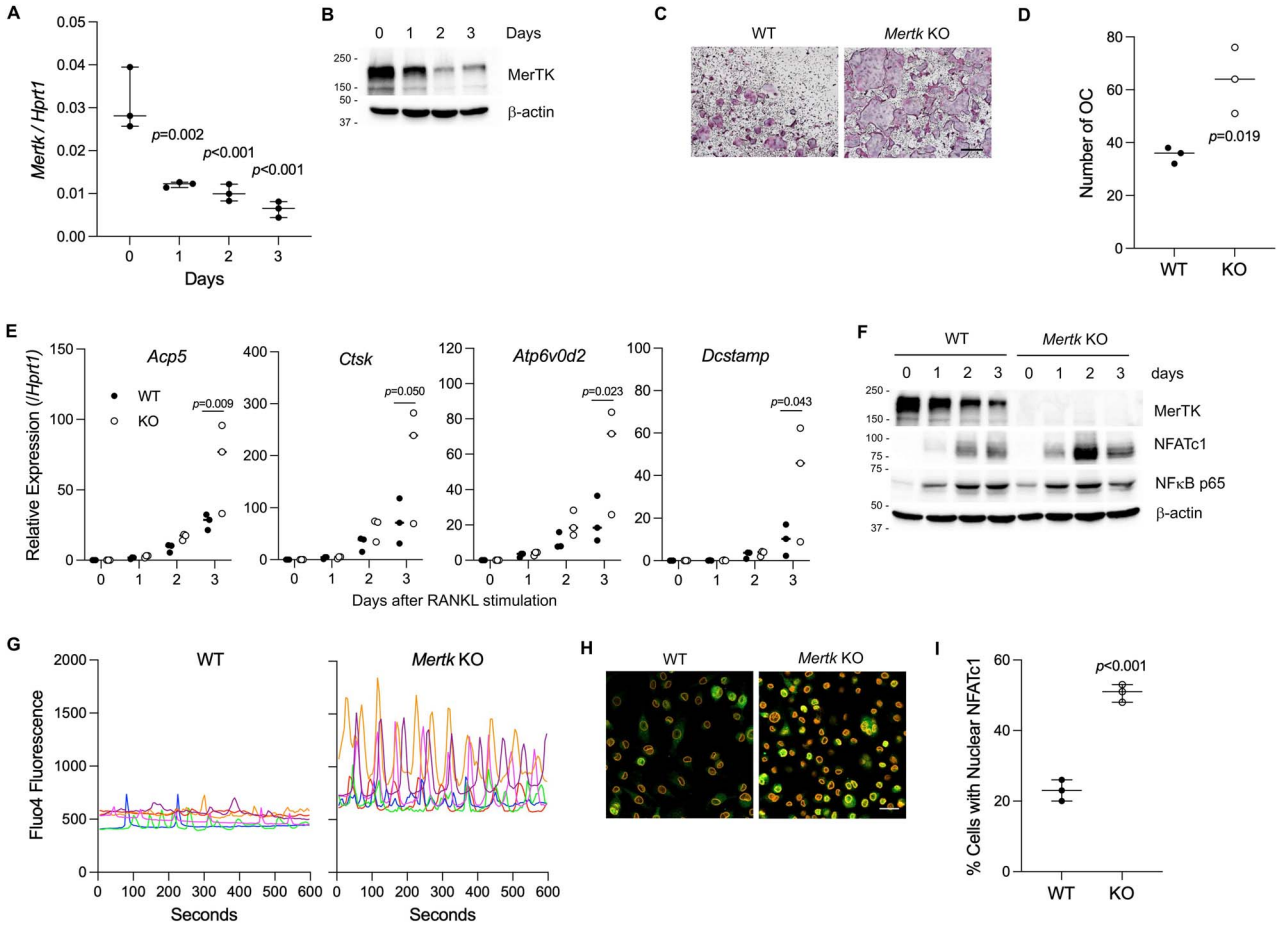

Figure 3. The role of MerTK in osteoclast differentiation. (A) WT BMMs were stimulated with 20 ng/mL M-CSF and 100 ng/mL RANKL for 3 d. The mRNA expression of *Mertk* was examined by real-time RT-PCR analysis. The F and *P*-values for one-way ANOVA analysis were 23.62 and .0002, respectively. (B) Cell lysates in (A) were subjected to western blotting for the expression of MerTK protein. (C) WT and Mertk KO BMMs were treated with 20 ng/mL M-CSF and 100 ng/mL RANKL for 4 d before staining for TRAP activity. Scale bar indicates 500 μm. (D) The number of TRAP-positive osteoclasts was counted from (C). (E) WT and *Mertk* KO BMMs were treated with 20 ng/mL M-CSF and 100 ng/mL RANKL for 3 d. The mRNA expression of osteoclast marker genes was measured by real-time RT-PCR analysis. Data are mean of three experiments performed in triplicates. The *P*-values for two-way ANOVA in the order of interaction, genotype, and RANKL stimulation were *Acp5* (.023, .018, <.001), *Ctsk* (.082, .048, <.001), *Atp6v0d2* (.48, .025, <.001), and *Dcstamp* (.056, .089, .002). (F) Cell lysates in (E) were subjected to western blotting for the expression of indicated proteins. (G) WT and *Mertk* KO BMMs were stimulated with 20 ng/mL M-CSF and 100 ng/mL RANKL for 2 d. The intracellular Ca^{2+}-dependent FLUO4 fluorescence was monitored for 10 min. Each line represents Ca^{2+} response of individual cell. The cells depicted in the graph were randomly selected among oscillating cells. (H) WT and KO BMMs grown on cover slips with 20 ng/mL M-CSF and 100 ng/mL RANKL for 2 d were immunostained with fluorescence-labeled antibodies against NFATc1 and Lamin B. Scale bar indicates 100 μm. (I) The number of cells exhibiting nuclear NFATc1 expression was counted from (H).

of the genotype of BMMs (Figure 4D). These results were further confirmed by use of a MerTK inhibitor, UNC 569,[24] during the co-culture of WT calvarial cells and bone marrow macrophages (Figure 4E). The inclusion of UNC 569 in the co-culture significantly reduced the number of TRAP-positive osteoclasts (Figure 4E and F), confirming the role of MerTK in osteoblast-dependent osteoclastogenesis. In consistence with the increased Opg/Rankl ratio in Mertk-deficient bones and calvarial cells, inhibition of MerTK by UNC 569 also resulted in a significant increase of *Opg/Rankl* mRNA expression in calvarial cells (Supplementary Figure S4C).

Mertk deficiency ameliorates bone resorption in periodontitis and ovariectomy

Since *Mertk* deficiency enhanced osteoblast differentiation and bone formation while reducing osteoclastogenesis, we next tested whether the altered bone metabolism in the absence of MerTK exert beneficial effect on the inflammatory bone loss using a mouse model of periodontitis. The placement of ligature around the second molar for 7 days induced significant loss of alveolar bones around the site in WT mice as shown in Figure 5A. In contrast, only modest bone loss was observed in *Mertk* KO mice following periodontitis induction. The measurement of the distance between cemento-enamel junction and alveolar bone crest clearly demonstrated severe bone loss in WT mice after ligation, while such bone erosion was significantly reduced in KO mice (Figure 5B). To confirm the role of osteoclasts in bone resorption in WT and KO mice, decalcified tissue sections were subjected to TRAP staining (Figure 5C). The significantly increased TRAP-stained area in alveolar bones after ligature in WT compared with only modest increase in KO bones corroborated the reduced periodontitis-induced bone resorption in the absence of MerTK. Histomorphometry analyses of osteoclast number per bone perimeter (N. OC/B. Pm, Figure 5D) and eroded surface per bone surface (ES/BS, Figure 5E) confirmed dramatic increase of osteoclasts and their activity in WT

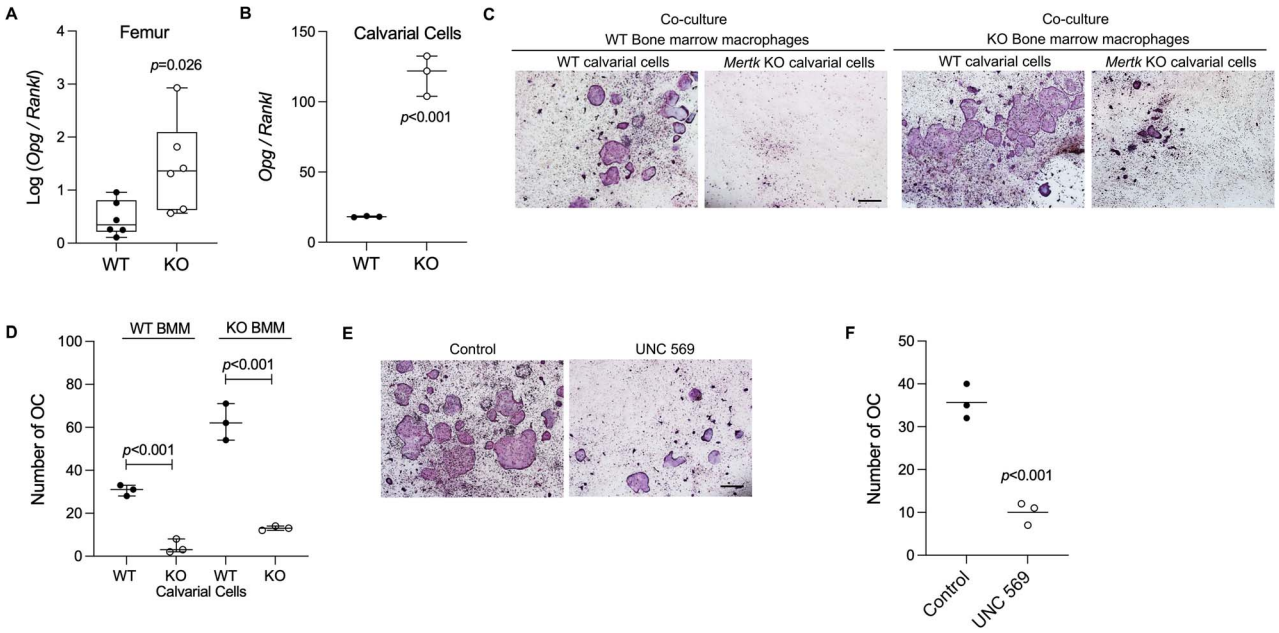

Figure 4. The effect of MerTK deficiency on osteoblast-dependent osteoclast differentiation. (A) The mRNA expression levels of Osteoprotegerin (*Tnfrsf11b*) and RANKL (*Tnfsf11*) in the femurs of WT and *Mertk* KO mice were measured by real-time RT-PCR analysis. The results were expressed as a ratio of 2 genes from individual mouse. (B) The mRNA expression of *Tnfrsf11b* and *Tnfsf11* was measured by real-time RT-PCR analysis in calvarial cells isolated from WT and *Mertk* KO mice. (C) WT of *Mertk* KO calvarial cells were co-cultured with WT or *Mertk*-deficient bone marrow macrophages in the presence of 10 nM vitamin D_3 and 1 μM PGE_2 for 7 d. Cells were stained for TRAP activity. Scale bar indicates 200 μm. (D) The number of TRAP-positive osteoclasts was counted from the results in (B). The *P*-values for two-way ANOVA in the order of interaction, calvarial cell genotype, and BMM genotype were (.003, <.001, <.001). (E) WT calvarial cells and bone marrow macrophages were co-cultured in the presence of vitamin D_3, PGE_2, and 20 nM UNC 569 (MerTK inhibitor) for 7 d followed by TRAP staining. Scale bar indicates 500 μm. (F) The number of osteoclasts was counted from the results in (E).

bones following ligature, while both the number of osteoclasts and bone erosion were significantly reduced in *Mertk* KO mice. The *Mertk* deficiency also affected microarchitecture of alveolar bones in the furcation area in addition to the alveolar bone height. As shown in the Supplementary Figure S5A, ligation induced significant resorption of the alveolar bones between the mesial and distal roots of molar 1 and molar 2 in WT mice. However, such dramatic loss of alveolar bones was not observed in KO mice after the induction of periodontitis. The analysis of BV/TV (Supplementary Figure S5B) and Tb. N (Supplementary Figure S5C) confirmed that the microarchitecture of alveolar bones in the furcation area were preserved following ligation in the absence of *Mertk*.

The role of *Mertk* during pathological bone resorption was further investigated in an ovariectomy-induced bone loss model in mice (Figure 6A). The bilateral ovariectomy induced significant trabecular bone loss in WT mice. Notably, the bone volume was significantly higher in *Mertk* KO mice compared with WT in both sham and ovariectomy groups. In accordance, the trabecular parameter of bone volume per tissue volume (Figure 6B) was significantly higher in *Mertk*-deficient mice compared with WT in both sham and ovariectomy groups with similar pattern observed in trabecular number (Figure 6C). To examine whether the decreased osteoclastogenesis in the absence of *Mertk* contributed to the reduced bone loss, femur sections were stained for TRAP activities (Figure 6D). The histomorphometry analyses revealed that both N. OC/B. Pm (Figure 6E) and ES/BS (Figure 6F) significantly increased following ovariectomy in WT mice. However, no such increase in the osteoclast number and activity were observed in ovariectomized *Mertk*-deficient mice. The reduced number and activity of osteoclasts corroborated the reduced serum CTX levels in KO mice compared with WT after ovariectomy (Figure 6G). Conversely, the serum levels of procollagen 1 N-terminal propeptide (P1NP) were consistently higher in KO mice compared with WT in both sham-operated and ovariectomized groups (Supplementary Figure S4B).

Discussion

MerTK is a member of TAM family receptor tyrosine kinases, the activity of which is mostly related to the clearance of apoptotic cells by phagocytosis, the regulation of innate immune responses, and cancer.[12,16] The physiological roles of MerTK are well-demonstrated in *Mertk* KO mice that exhibited dramatically reduced phagocytosis of apoptotic thymocytes by macrophages.[15] These mice were susceptible to the LPS-induced endotoxic shock with concomitantly increased TNF-α production compared with WT mice.[13] In addition, pathologic roles of MerTK are found in numerous leukemias as well as in solid tumors that the aberrant expression of the protein endows cell proliferation and survival leading to the carcinogenesis.[25–27] In the present study, we demonstrated novel bone phenotype of *Mertk* KO mice. Compared with littermate controls, *Mertk* KO femurs exhibited dramatically increased trabecular bone volume accompanied by increased number of osteoblasts and the rate of bone formation, with concomitant decrease of osteoclast number (Figure 1). The increase in the bone volume was also observed in trabecular bones in vertebral bodies, suggesting a global role of *Mertk* in regulating both limb and axial

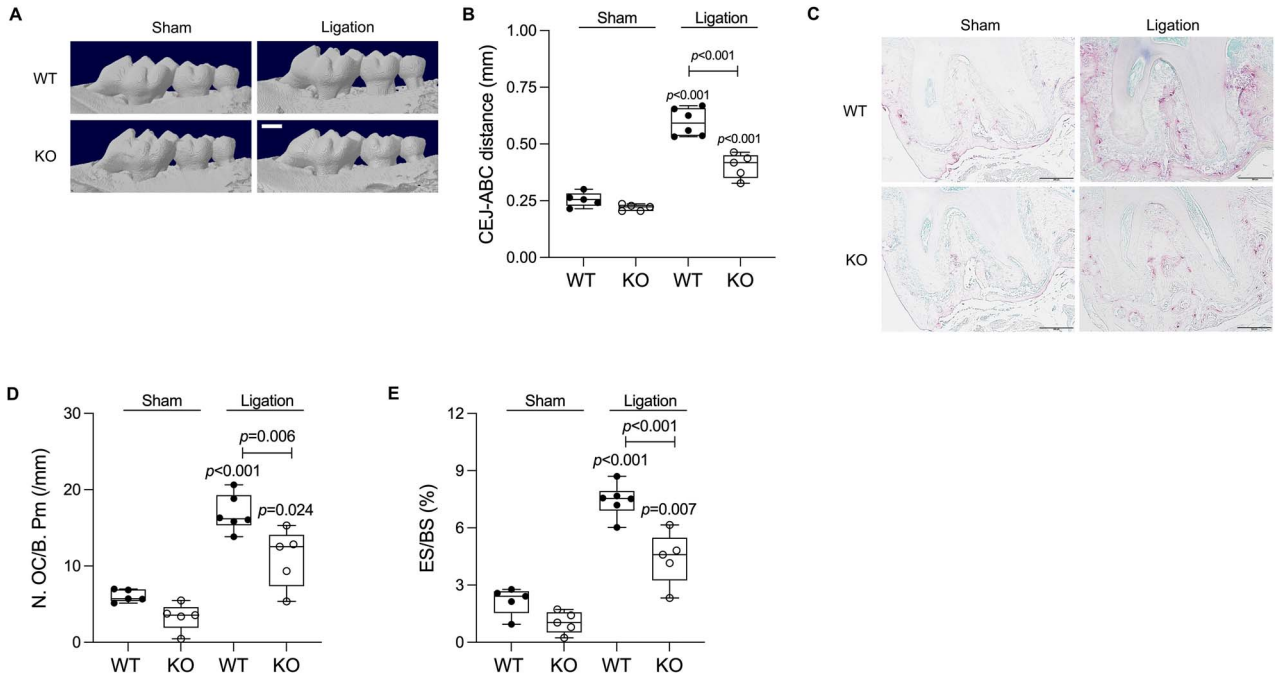

Figure 5. The effect of *Mertk* deficiency on periodontitis-induced alveolar bone resorption. (A) The left maxillary second molar of 8-wk-old male WT and *Mertk* KO mice were ligated for 7 d to induce periodontitis. The tissue samples were subjected to microcomputed tomography analysis, and the data were reconstructed for 3-dimensional visualization. Scale bar indicates 500 μm. (B) The distance between cemento-enamel junction and alveolar bone crest was measured from the results in (A). The *P*-values for two-way ANOVA in the order of interaction, genotype, and ligature were (.001, <.001, <.001). (C) Tissue sections from experiments in (A) were subjected to TRAP staining. Scale bar indicates 200 μm. (D and E) The number of osteoclasts per bone perimeter and eroded surface per bone surface were calculated from the results in (C). The *P*-values for two-way ANOVA in the order of interaction, genotype, and ligature were N. OC/B. Pm (.176, .001, <.001) and ES/BS (.032, <.001, <.001).

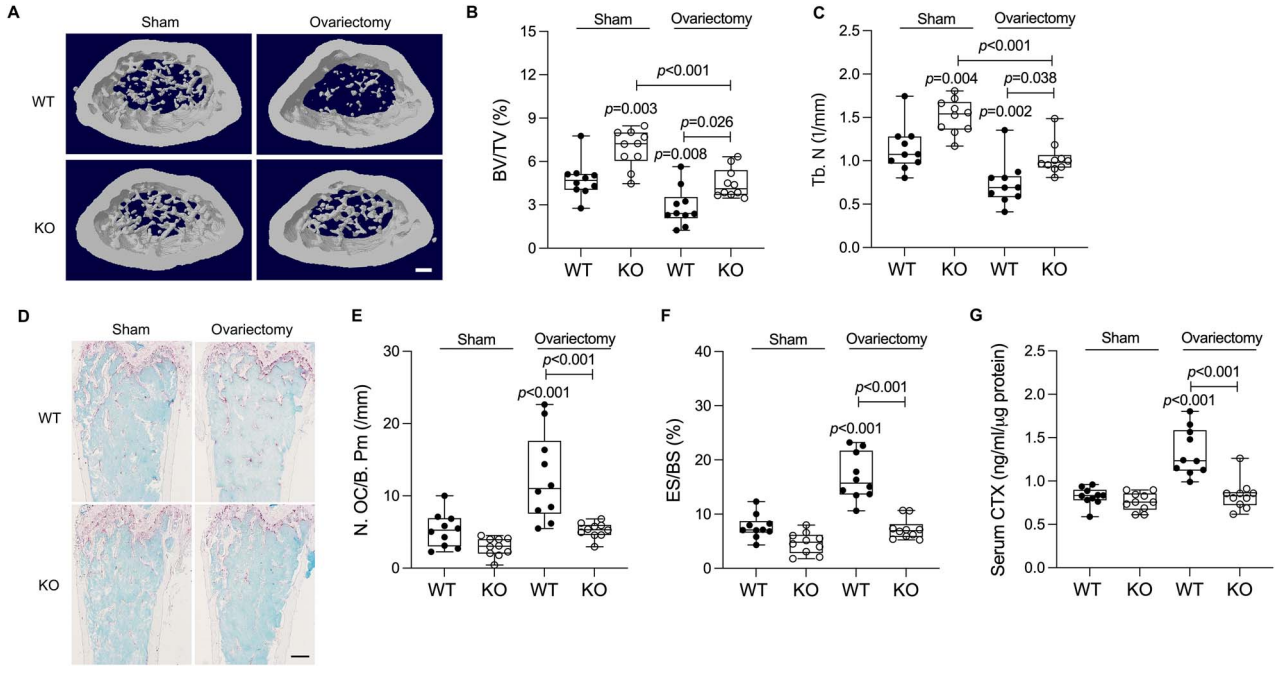

Figure 6. The effect of *Mertk* deficiency on ovariectomy-induced bone resorption. (A) Twelve-week-old female WT and *Mertk* KO mice were bilaterally ovariectomized. At 4 wks after operation, femur samples were subjected to microcomputed tomography analysis, and the data were reconstructed for 3-dimensional visualization. Scale bar indicates 200 μm. (B) The trabecular bone volume per tissue volume was calculated from the data in (A). (C) The trabecular number was calculated from the data in (A). The *P*-values for two-way ANOVA in the order of interaction, genotype, and ovariectomy were BV/TV (.544, <.001, <.001) and Tb. N (.540, <.001, <.001). (D) The femur sections from the experiments in (A) were subjected to TRAP staining followed by methyl green counterstaining. Scale bar indicates 200 μm. (E and F) The number of osteoclasts per bone perimeter and eroded surface per bone surface were calculated from the results in (D). The *P*-values for two-way ANOVA in the order of interaction, genotype, and ovariectomy were N. OC/B. Pm (.027, <.001, <.001) and ES/BS (<.001, <.001, <.001). (G) The serum levels of CTX were examined by ELISA. The results were normalized by protein concentrations in the sera. The *P*-values for two-way ANOVA in the order of interaction, genotype, and ovariectomy were (<.001, <.001, <.001).

skeletons. However, the limitation of current study is that the bone metabolism was only assessed in young adults. Thus, further studies are required to fully understand the role of *Mertk* in bone metabolism including the age-related changes. While this manuscript was in preparation, Engelmann et al. published that *Col1a1* promoter–driven deletion of *Mertk* induced the increase of tibia trabecular bone density in mice,[28] which was in agreement with our results. The increased bone formation was due to the intrinsic increase of osteogenic activity of osteoblast precursors, since stimulation of calvarial cells from *Mertk* KO mice resulted in dramatically enhanced ALP activity, mineralization, and expression of osteoblast marker genes (Figure 2).

The *Mertk* deficiency in osteoblast precursors rendered significant stimulation of several key regulatory signaling pathways in osteoblast differentiation. The canonical Wnt signaling pathway is crucial for the maintenance of bone mass by directly regulating osteoblast differentiation.[29–31] In *Mertk* KO calvarial cells, significantly increased expression of β-catenin accompanied by increased phosphorylation of GSK3β was observed in response to culture with BMP2 for at least 4 d (Figure 2D and E). Upon binding of BMPs on osteoblast precursors, Smad signaling crucially translates ligand binding to osteogenic gene expression, for example, *Runx2*.[32] The BMP2 induced markedly higher phosphorylation of Smad1/5/8 in *Mertk* KO cells compared with control, conforming to the increased osteogenic activity. Interestingly, BMP2 stimulation for 30 min did not alter β-catenin expression, GSK3β, or Smad1/5/8 phosphorylation (Supplementary Figure S2E), suggesting potential involvement of transcriptional regulations. In this context, we observed considerable increase in the expression of *Smad4* with conspicuous reduction in *Nog* expression in KO calvarial cells compared with WT at 7 d after BMP2 stimulation (Supplementary Tables 1 and 2) using an RT-PCR–based array analysis (Supplementary Figure S5). It has been reported that Smad4 is required for BMP2-dependent osteoblast differentiation and mineralization,[33,34] while the overexpression of Noggin, a BMP antagonist, reduced osteoblast differentiation and bone formation in mice.[35] Notably, BMP2 induces Wnt3a expression in osteogenic cells,[36] while Wnt/β-catenin signaling stimulates BMP2 expression.[37] Taken together, these results raise a possibility that β-catenin and Smad pathways might cooperate to enhance osteogenic differentiation in *Mertk* KO osteoblast precursors. Furthermore, the expression of NFATc1 was also significantly increased in *Mertk* KO cells after BMP2 stimulation. Importantly, transgenic mice expressing constitutively active NFATc1 exhibited significantly increased osteoblast proliferation, bone formation, and bone volume.[38] Introduction of additional copy of *Dyrk1a* gene, the product of which phosphorylates and inactivates NFATc1, resulted in reduced osteoblast differentiation and bone formation in mice.[39] Thus, it is likely that NFATc1 might be one of the downstream targets of MerTK involved in the regulation of bone metabolism. However, how the *Mertk* deficiency stimulates these regulatory signaling pathways of osteoblast differentiation could not be determined in the current experiments, which might be an interesting subject of further studies.

Another notable role of MerTK in bone metabolism discovered in the current study is the regulation of osteoclastogenesis. The absence of *Mertk* endowed BMMs with significantly increased osteoclastogenic potential (Figure 3), in contrast to the conspicuously decreased osteoclast number in bone tissues (Figure 1). The dramatic increase of intracellular Ca^{2+} oscillations, NFATc1 expression, and its nuclear localization suggested that the augmented Ca^{2+}-NFATc1 signaling axis plays a key role in the enhanced differentiation potential of the osteoclast precursors. However, the absence of *Mertk* significantly elevated the *Opg/Rankl* ratio in bones and osteoblast precursors (Figure 4), likely causing the reduced osteoclastogenesis in vivo and osteoblast-osteoclast co-cultures (Figures 1 and 4). As far as we know, no study has been reported regarding the role of MerTK on *Tnfrsf11b* expression. In the present report, we showed that *Mertk* deficiency significantly increased Smad1/5/8 phosphorylation (Figure 2D and E) and *Smad4* expression (Supplementary Table S1). Interestingly, the proximal region of human *TNFRSF11B* promoter contained Smad binding element[40] that is activated by Smad4-containing complexes.[41] Thus, it is likely that the increased BMP signaling in the absence of *Mertk* induced *Tnfrsf11b* expression in our experiments.

Aberrantly increased osteoclast number and activity are responsible for severe destruction of alveolar bones found in periodontitis. Indeed, periodontitis is a major cause of adult tooth loss.[10,11] In addition, numerous studies indicate that periodontitis is also associated with other systemic diseases.[8,42] However, currently no antiresorptive therapy is available to prevent alveolar bone loss in periodontitis. Here, the absence of *Mertk* ameliorated alveolar bone loss in a mouse model of periodontitis. Furthermore, the role of MerTK in bone resorption was further confirmed in ovariectomized mice. In addition, a MerTK inhibitor UNC 569 exhibited significant inhibition of osteoclastogenesis while increasing osteoblast differentiation suggesting that targeting MerTK might be a plausible strategy against inflammation-induced and hormone-deprival–induced bone lysis. Thus, it is likely that the inhibition of MerTK activity/expression might exhibit dual benefits of enhancing bone formation while reducing bone resorption in conditions of pathological bone loss. Yet, it should be noted that some repercussions were reported in *Mertk*-deficient mice including retinal dystrophy, susceptibility to LPS-induced endotoxic shock, and defective phagocytosis.[12–15] Indeed, one study indicated potential adverse effect of UNC 569 on the phagocytic function of retinal pigment epithelial cells,[43] suggesting that caution is need when developing drug candidates that inhibit MerTK activity. To conclude, this study reported novel role of MerTK in bone metabolism by showing the increased bone density in both axial and limb skeletons of male and female *Mertk*-deficient mice, due to increased bone formation and decreased bone resorption. The bone-protective effect of *Mertk* deficiency in the ligature- and ovariectomy-induced models of bone lysis suggests potential development of MerTK inhibitors as drug candidates for osteolytic diseases such as periodontitis and osteoporosis.

Author contributions

Ka-Young Ryu (Data curation, Investigation, Validation, Formal analysis, Writing—original draft), Nitin Kumar Pokhrel (Investigation, Data curation, Formal analysis, Visualization, Writing—original draft), Hye-Jin Jung (Data curation, Investigation, Visualization, Writing—original draft, Formal analysis), Hyo Jeong Kim (Data curation, Investigation, Writing—review & editing), Jiwon Seok (Data

curation, Investigation, Writing—review & editing), Tae-Young Kim (Data curation, Investigation, Writing—review & editing), Hyung Joon Kim (Methodology, Investigation, Writing—review & editing), Ji Hye Lee (Methodology, Investigation, Writing—review & editing), Jae-Young Kim (Writing—review & editing, Investigation), Yong-Gun Kim (Investigation, Methodology, Writing—review & editing, Conceptualization), Youngkyun Lee (Conceptualization, Data curation, Investigation, Formal analysis, Supervision, Funding acquisition, Visualization, Writing—review & editing, Writing—original draft, Project administration)

Supplementary material

Supplementary material is available at *JBMR Plus* online.

Funding

This work was supported by grants from the National Research Foundation of Korea funded by the Ministry of Science, ICT, and Future Planning (Y.L., NRF-2020R1A2C1009364 and NRF-2017R1A5A2015391).

Conflicts of interest

All the authors state that they have no conflicts of interests.

Data availability

The data that support the findings of this study are available from the corresponding author upon reasonable request.

References

1. Hadjidakis DJ, Androulakis II. Bone remodeling. *Ann N Y Acad Sci*. 2006;1092(1):385–396. https://doi.org/10.1196/annals.1365.035.
2. Bolamperti S, Villa I, Rubinacci A. Bone remodeling: an operational process ensuring survival and bone mechanical competence. *Bone Res*. 2022;10(1):48. https://doi.org/10.1038/s41413-022-00219-8.
3. Takahashi N, Akatsu T, Udagawa N, et al. Osteoblastic cells are involved in osteoclast formation. *Endocrinology*. 1988;123(5):2600–2602. https://doi.org/10.1210/endo-123-5-2600.
4. Udagawa N, Takahashi N, Yasuda H, et al. Osteoprotegerin produced by osteoblasts is an important regulator in osteoclast development and function. *Endocrinology*. 2000;141(9):3478–3484. https://doi.org/10.1210/endo.141.9.7634.
5. Nakashima T, Hayashi M, Fukunaga T, et al. Evidence for osteocyte regulation of bone homeostasis through RANKL expression. *Nat Med*. 2011;17(10):1231–1234. https://doi.org/10.1038/nm.2452.
6. Xiong J, Onal M, Jilka RL, Weinstein RS, Manolagas SC, O'Brien CA. Matrix-embedded cells control osteoclast formation. *Nat Med*. 2011;17(10):1235–1241. https://doi.org/10.1038/nm.2448.
7. Tsukasaki M, Asano T, Muro R, et al. OPG production matters where it happened. *Cell Rep*. 2020;32(10):108124. https://doi.org/10.1016/j.celrep.2020.108124.
8. Hajishengallis G. Periodontitis: from microbial immune subversion to systemic inflammation. *Nat Rev Immunol*. 2015;15(1):30–44. https://doi.org/10.1038/nri3785.
9. Bartold PM, Cantley MD, Haynes DR. Mechanisms and control of pathologic bone loss in periodontitis. *Periodontology*. 2000;53(1):55–69. https://doi.org/10.1111/j.1600-0757.2010.00347.x.
10. Oliver RC, Brown LJ. Periodontal diseases and tooth loss. *Periodontology*. 2000;2(1):117–127. https://doi.org/10.1111/j.1600-0757.1993.tb00224.x.
11. Papapanou PN. Periodontal diseases: epidemiology. *Ann Periodontol*. 1996;1(1):1–36. https://doi.org/10.1902/annals.1996.1.1.1.
12. Lemke G. Biology of the TAM receptors. *Cold Spring Harb Perspect Biol*. 2013;5(11):a009076. https://doi.org/10.1101/cshperspect.a009076.
13. Camenisch TD, Koller BH, Earp HS, Matsushima GK. A novel receptor tyrosine kinase, Mer, inhibits TNF-alpha production and lipopolysaccharide-induced endotoxic shock. *J Immunol*. 1999;162(6):3498–3503. https://doi.org/10.4049/jimmunol.162.6.3498.
14. Duncan JL, LaVail MM, Yasumura D, et al. An RCS-like retinal dystrophy phenotype in mer knockout mice. *Invest Ophthalmol Vis Sci*. 2003;44(2):826–838. https://doi.org/10.1167/iovs.02-0438.
15. Scott RS, McMahon EJ, Pop SM, et al. Phagocytosis and clearance of apoptotic cells is mediated by MER. *Nature*. 2001;411(6834):207–211. https://doi.org/10.1038/35075603.
16. Huelse JM, Fridlyand DM, Earp S, DeRyckere D, Graham DK. MERTK in cancer therapy: targeting the receptor tyrosine kinase in tumor cells and the immune system. *Pharmacol Ther*. 2020;213:107577. https://doi.org/10.1016/j.pharmthera.2020.107577.
17. Lu Q, Gore M, Zhang Q, et al. Tyro-3 family receptors are essential regulators of mammalian spermatogenesis. *Nature*. 1999;398(6729):723–728. https://doi.org/10.1038/19554.
18. Kilkenny C, Browne WJ, Cuthill IC, Emerson M, Altman DG. Improving bioscience research reporting: the ARRIVE guidelines for reporting animal research. *PLoS Biol*. 2010;8(6):e1000412. https://doi.org/10.1371/journal.pbio.1000412.
19. Kim HJ, Ryu KY, Kim YG, et al. Myeloid-specific PTP1B deficiency attenuates inflammation-induced and ovariectomy-induced bone loss in mice by inhibiting osteoclastogenesis. *J Bone Miner Res*. 2022;37(3):505–514. https://doi.org/10.1002/jbmr.4478.
20. Abe T, Hajishengallis G. Optimization of the ligature-induced periodontitis model in mice. *J Immunol Methods*. 2013;394(1–2):49–54. https://doi.org/10.1016/j.jim.2013.05.002.
21. Dempster DW, Compston JE, Drezner MK, et al. Standardized nomenclature, symbols, and units for bone histomorphometry: a 2012 update of the report of the ASBMR Histomorphometry nomenclature committee. *J Bone Miner Res*. 2013;28(1):2–17. https://doi.org/10.1002/jbmr.1805.
22. Asagiri M, Sato K, Usami T, et al. Autoamplification of NFATc1 expression determines its essential role in bone homeostasis. *J Exp Med*. 2005;202(9):1261–1269. https://doi.org/10.1084/jem.20051150.
23. Takayanagi H, Kim S, Koga T, et al. Induction and activation of the transcription factor NFATc1 (NFAT2) integrate RANKL signaling in terminal differentiation of osteoclasts. *Dev Cell*. 2002;3(6):889–901. https://doi.org/10.1016/S1534-5807(02)00369-6.
24. Liu J, Yang C, Simpson C, et al. Discovery of novel small molecule Mer kinase inhibitors for the treatment of Pediatric acute lymphoblastic Leukemia. *ACS Med Chem Lett*. 2012;3(2):129–134. https://doi.org/10.1021/ml200239k.
25. Cummings CT, Deryckere D, Earp HS, Graham DK. Molecular pathways: MERTK signaling in cancer. *Clin Cancer Res*. 2013;19(19):5275–5280. https://doi.org/10.1158/1078-0432.CCR-12-1451.
26. Burstyn-Cohen T, Maimon A. TAM receptors, phosphatidylserine, inflammation, and cancer. *Cell Commun Signal*. 2019;17(1):156. https://doi.org/10.1186/s12964-019-0461-0.
27. Wu G, Ma Z, Cheng Y, et al. Targeting Gas6/TAM in cancer cells and tumor microenvironment. *Mol Cancer*. 2018;17(1):20. https://doi.org/10.1186/s12943-018-0769-1.

28. Engelmann J, Zarrer J, Gensch V, et al. Regulation of bone homeostasis by MERTK and TYRO3. *Nat Commun*. 2022;13(1):7689. https://doi.org/10.1038/s41467-022-33938-x.
29. Duan P, Bonewald LF. The role of the wnt/beta-catenin signaling pathway in formation and maintenance of bone and teeth. *Int J Biochem Cell Biol*. 2016;77(Pt A):23–29. https://doi.org/10.1016/j.biocel.2016.05.015.
30. Baron R, Kneissel M. WNT signaling in bone homeostasis and disease: from human mutations to treatments. *Nat Med*. 2013;19(2):179–192. https://doi.org/10.1038/nm.3074.
31. Glass DA 2nd, Karsenty G. Molecular bases of the regulation of bone remodeling by the canonical Wnt signaling pathway. *Curr Top Dev Biol*. 2006;73:43–84
32. Wu M, Chen G, Li YP. TGF-beta and BMP signaling in osteoblast, skeletal development, and bone formation, homeostasis and disease. *Bone Res*. 2016;4(1):16009. https://doi.org/10.1038/bonekey.2016.9.
33. Karner CM, Lee SY, Long F. Bmp induces osteoblast differentiation through both Smad4 and mTORC1 signaling. *Mol Cell Biol*. 2017;37(4):e00253–16. https://doi.org/10.1128/MCB.00253-16.
34. Tan X, Weng T, Zhang J, et al. Smad4 is required for maintaining normal murine postnatal bone homeostasis. *J Cell Sci*. 2007;120(13):2162–2170. https://doi.org/10.1242/jcs.03466.
35. Wu XB, Li Y, Schneider A, et al. Impaired osteoblastic differentiation, reduced bone formation, and severe osteoporosis in noggin-overexpressing mice. *J Clin Invest*. 2003;112(6):924–934. https://doi.org/10.1172/JCI15543.
36. Rawadi G, Vayssiere B, Dunn F, Baron R, Roman-Roman S. BMP-2 controls alkaline phosphatase expression and osteoblast mineralization by a Wnt autocrine loop. *J Bone Miner Res*. 2003;18(10):1842–1853. https://doi.org/10.1359/jbmr.2003.18.10.1842.
37. Zhang R, Oyajobi BO, Harris SE, et al. Wnt/beta-catenin signaling activates bone morphogenetic protein 2 expression in osteoblasts. *Bone*. 2013;52(1):145–156. https://doi.org/10.1016/j.bone.2012.09.029.
38. Winslow MM, Pan M, Starbuck M, et al. Calcineurin/NFAT signaling in osteoblasts regulates bone mass. *Dev Cell*. 2006;10(6):771–782. https://doi.org/10.1016/j.devcel.2006.04.006.
39. Lee Y, Ha J, Kim HJ, et al. Negative feedback inhibition of NFATc1 by DYRK1A regulates bone homeostasis. *J Biol Chem*. 2009;284(48):33343–33351. https://doi.org/10.1074/jbc.M109.042234.
40. Thirunavukkarasu K, Miles RR, Halladay DL, et al. Stimulation of osteoprotegerin (OPG) gene expression by transforming growth factor-β (TGF-β). Mapping of the OPG promoter region that mediates TGF-β effects. *J Biol Chem*. 2001;276(39):36241–36250. https://doi.org/10.1074/jbc.M104319200.
41. Jonk LJ, Itph S, Heldin CH, ten Djike P, Kruijer W. Identification and functional characterization of a Smad binding element (SBE) in the JunB promoter that acts as a transforming growth factor-beta, activin, and bone morphogenetic protein-inducible enhancer. *J Biol Chem*. 1998;273(33):21145–21152. https://doi.org/10.1074/jbc.273.33.21145.
42. Hajishengallis G, Chavakis T. Local and systemic mechanisms linking periodontal disease and inflammatory comorbidities. *Nat Rev Immunol*. 2021;21(7):426–440. https://doi.org/10.1038/s41577-020-00488-6.
43. Sayama A, Okado K, Nakamura K, et al. UNC569-induced morphological changes in pigment epithelia and photoreceptor cells in the retina through MerTK inhibition in mice. *Toxicol Pathol*. 2018;46(2):193–201. https://doi.org/10.1177/0192623317749469.